Geosciences Journal
Vol. 20, No. 2, p. 167 − 182, April 2016
DOI 10.1007/s12303-015-0043-0

Spectral characteristics of minerals associated with skarn deposits: a case study of Weondong skarn deposit, South Korea

Yongsik Jeong *Department of Astronomy, Space Science and Geology, Chungnam National University, Daejeon 305-764, Republic of Korea*
Jaehyung Yu* *Department of Geology and Earth Environmental Sciences, Chungnam National University, Daejeon 305-764, Republic of Korea*
Sang-Mo Koh, Chul-Ho Heo *Mineral Resources Research Division, Korea Institute of Geoscience and Mineral Resources, Daejeon 305-350, Republic of Korea*
Jeonga Lee *Department of Astronomical Science and Geology, Chungnam National University, Daejeon 305-764, Republic of Korea*

ABSTRACT: This study examined the spectral characteristics of minerals occurring at Weondong skarn deposit located in South Korea and assessed the effectiveness of VNIR-SWIR spectroscopic approaches in zone definition characterizing skarn deposits based on XRD, XRF, and petrographic studies. The spectroscopic analyses identified intrusive rock, garnet-clinopyroxene skarn, clinopyroxene-garnet skarn, W-ore, and host rock zones. The assessment results for VNIR-SWIR spectroscopy in skarn exploration illustrated that the spectral approaches would be very useful for attaining skarn mineral information such as calcite, chlorite, clinopyroxene, garnet, scapolite, vesuvianite, and wollastonite and clay minerals. Furthermore, the rock-forming minerals such as K-feldspar, plagioclase, quartz, fluorite, and tungsten-bearing minerals like scheelite may require supplementary mineral analysis. A combined analysis of spectrometry, XRD, XRF, UV lamp scanning, and petrographic studies reveals that the skarn mineralization of the study area related to W mineral of the study core is defined as proximal endoskarn to proximal exoskarn, which could be defined by spectroscopic approaches.

Key words: spectral characteristics, skarn deposit, assessment, VNIR-SWIR spectroscopy, mineral exploration

1. INTRODUCTION

After the development of a portable spectrometer, spectroscopic approaches in mineral exploration have become widely known as one of the most useful tools for mineral exploration due to their convenience with lower costs and rapidity in mineral identification. In general, VNIR-SWIR spectroscopic approaches depend on the absorption features by the color variations or molecular changes in the minerals (Thomson et al., 1990; Kerr et al., 2011). The absorption features of the VNIR region (400–1300 nm) are commonly related to specific minerals including metals (Fe, Ni, Cr, and Mn-bearing minerals). The VNIR spectroscopy is known as to identify iron oxyhydroxides including jarosite, hematite, goethite, and schwertmannite (Hauff, 2008), and Fe containing hydroxylated silicates such as chlorite, biotite, epidote, iron carbonates, pyroxene, and olivines (Pontual et al., 2012). In addition, the spectral characteristics of SWIR region (1300–2500 nm) are typically related to the molecular bond vibration of hydroxyl (OH), water (H_2O), carbonates ($CO\cdot$), and cation-OH bonds (e.g., Al-OH, Mg-OH, and Fe-OH) (Thomson et al., 1990; Hauff, 2008; Kerr et al., 2011; Pontual et al., 2012). Due to their relationship between molecular bond vibration and the spectral characteristics, SWIR spectroscopy is widely used for detection of major alteration minerals such as clays, white micas (illite, muscovite), chlorite, hydroxides, zeolites, and carbonates (Herrmann et al., 2001; Hauff, 2008; Pontual et al., 2012).

There have been many studies employing field spectroscopic approaches in mineral exploration (Thomson et al., 1999; Yang et al., 2000; Sun et al., 2001; Yang et al., 2001; Kerr et al., 2011; Sonntag et al., 2012; Zadeh et al., 2014). Previous studies on mineral exploration using spectroscopy are almost focused on alteration zone mapping of hydrothermal deposits based on shortwave infrared (SWIR hereafter) spectroscopy (Thompson et al., 1999; Sun et al., 2001; Kerr et al., 2011; Sonntag et al., 2012), and the classification of alteration mineral assemblages of porphyry copper deposits on the basis of visible-near infrared (VNIR hereafter) and SWIR regions (Zadeh et al., 2014).

On the other hand, efforts to assess the effectiveness of spectroscopic approaches in mineral exploration are also being made. Yang et al. (2000) and Yang et al. (2001) compared SWIR spectroscopic results with the previously published data for geothermal systems and verified the effectiveness of SWIR spectroscopic approaches in geothermal systems mainly based on clay minerals. Moreover, a few studies tried to compare SWIR spectroscopic results with XRD and XRF results (Sun et al., 2001) or XRD and petrographic analyses (Sonntag et al., 2012) for hydrothermal alteration minerals of low-sulfidation epithermal systems and concluded that spectroscopic approaches were effective in the detection of clay minerals, white mica, and chorite-epidote composition.

Although previous researchers have investigated application cases of alteration zone mapping using VNIR and SWIR spec-

*Corresponding author: jaeyu@cnu.ac.kr

troscopy and the effectiveness of SWIR spectroscopy in hydrothermal alteration, none to date have assessed the usefulness of VNIR and SWIR spectroscopy for skarn investigation other than Jeong et al. (2014). Moreover, skarn deposits are one of the more abundant ore types in the earth's crust and form in rocks of almost all ages, and the major skarn types are related to the key materials such as Fe, Au, Cu, Zn, W, Mo, and Sn, which can be economically important (Meinert et al., 2005). Moreover, skarn deposits also have alteration zones and general patterns are comprised of proximal garnet, distal pyroxene, and skarn minerals like wollastonite, vesuvianite, sulfides, and oxides (Meinert et al., 2005). If the types of skarn mineralization and zoning patterns can be identified in the field conveniently using spectroscopy, it would contribute significantly in skarn deposit exploration.

This study evaluated the efficiency of VNIR-SWIR spectroscopic approaches for the field exploration in defining intrusive rock, skarn zonation, mineralization, and wall rock distribution for a skarn ore deposit located in South Korea by comparing spectroscopic characteristics with XRD, XRF, and petrographic studies.

2. GEOLOGY AND MINERALIZATION

The Weondong deposit is a skarn-type deposit located in the northeast part of South Korea, which is about 190 km East from Seoul (Fig. 1). The geology of this deposit area is represented by Cambro-Ordovician Maggol Limestone intruded by Cretaceous rhyolite/quartz porphyry (Fig. 1) (Hwang, 1997; Chi et al., 2011; Lee, 2011). Maggol Limestone consists mainly of limestones interbedded with thin layers of shale and slate. Cretaceous rhyolite/quartz porphyry stock intrudes Maggol Limestone in a N45–60°E direction (Chi et al., 2011). However, the sill-type intrusion of the quartz porphyry to Maggol Limestone is often observed with a thickness of approximately 100 m around 150 m in depth (Chi et al., 2011). The W ore is developed along the bedding plane of Maggol Limestone and a fissure zone developed along the contact between Maggol Limestone and the quartz porphyry (Chi et al., 2012). The rhyolite/quartz porphyry interacted with Maggol Limestone developing skarn mineralization and hydrothermal alteration over the rhyolite/quartz porphyry and the limestone (Hwang and Lee, 1998). The major structure of the study area consists of a thrust fault with a strike of N40–50°E with minor fractures (Fig. 1) (Chi et al., 2011). These structures are considered the main conduits for the ore-forming fluids responsible for the mineralization of the Weondong deposit (Lee, 2011).

There are three metallic mineralizations reported to be associated with the skarn; Pb-Zn, Fe, and W-Mo (Lee, 2011). The mineralization and skarn zones occur widely over both Maggol Limestone and rhyolite/quartz porphyry where the

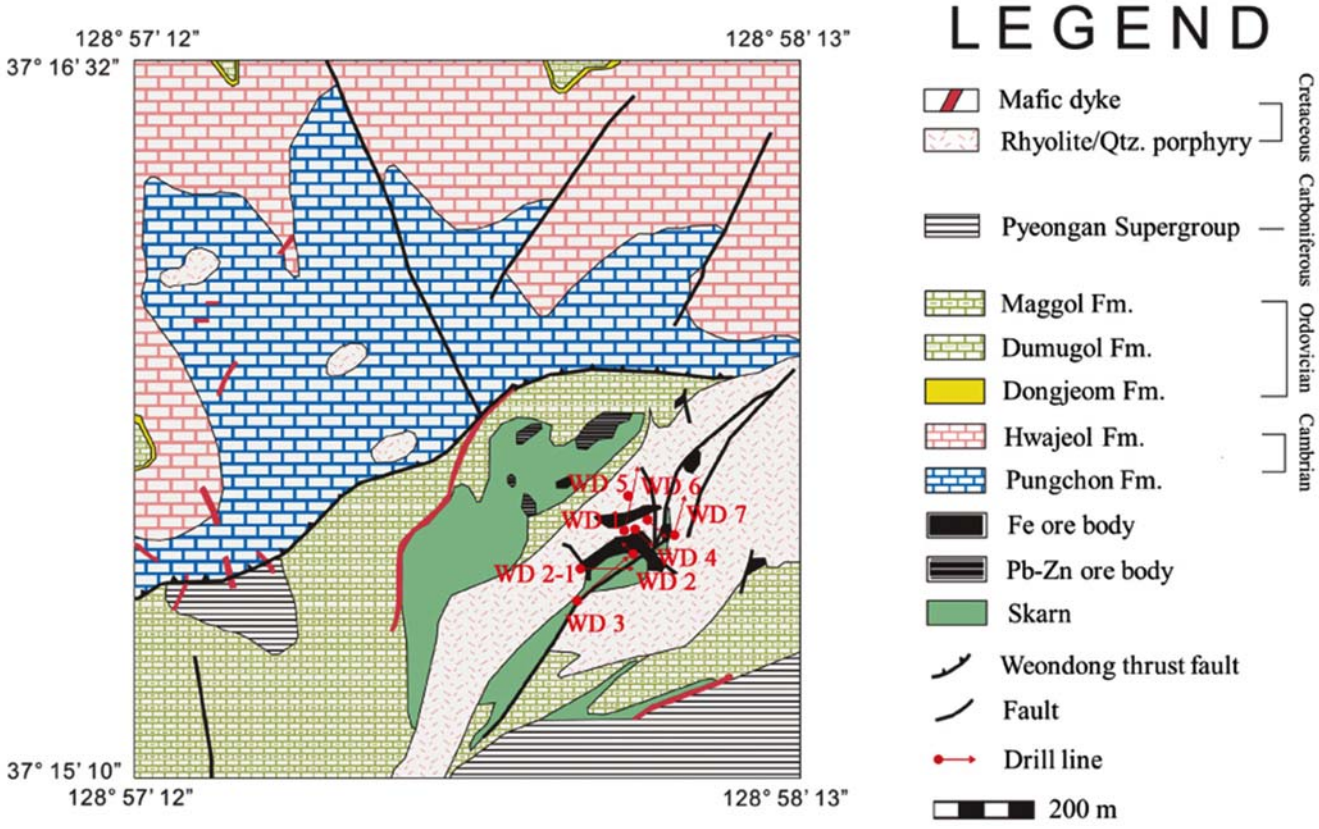

Fig. 1. Location map and simplified geologic map for the Weondong deposit area showing a total of 8 drill-hole locations (revised from Lee, 2011).

limestone skarn zone is related to the Pb-Zn-Fe mineralization, and the rhyolite/quartz porphyry skarn zone is associated with the W-Mo mineralization (Lee, 2011). A previous study subdivided the skarn and mineralized zones into garnet-clinopyroxene, clinopyroxene-garnet, W-ore, magnetite, and Pb-Zn ore zones based on the skarn and ore mineral assemblages (Park et al., 2013). Skarn minerals reported from previous studies are amphibolite, calcite, chlorite, clinopyroxene, epidote, fluorite, garnet, phlogopite, scheelite, and vesuvianite (Hwang and Lee, 1998; Chi et al., 2012).

3. METHODS

To assess effectiveness of spectroscopic approaches in field skarn exploration, we selected the most appropriate drill hole (WD-2-1) for the study area. To simulate the field exploration, spectroscopic analysis in high resolution in terms of spectra measurement interval was firstly conducted. The results from spectroscopic analyses were cross-validated with mineralogical analyses including XRD, XRF, and petrographic study to assess its effectiveness in skarn exploration. Detail core logging inferring characteristics of the ore geology for a skarn ore deposit is constructed (Fig. 2).

3.1. Sample Core Selection

The Korea Institute of Geoscience and Mineral Resources (KIGAM hereafter) executed drilling exploration of Weondong deposit to understand the extent of the W-ore body, and a total of 8 drill holes were produced (Fig. 1). Among the 8 drill holes, this study chose the WD-2-1 drill hole to assess the effectiveness of spectroscopic approaches in mineral exploration based on core inclination, core length, ore body length, and the coverage of various mineral and host rock distributions. The WD-2-1 has a length of 400 m with an inclination angle of 80°, which covers 174.95 m of ore (Chi et al., 2012). Moreover, WD-2-1 includes intrusive rock (quartz porphyry) as a sill shape, host rock (Maggol Limestone), the W-ore zone, and two different types of skarn zones, which make it the most appropriate for the assessment of spectroscopic approaches (Chi et al., 2012).

3.2. VNIR-SWIR Spectroscopy

VNIR-SWIR spectral measurement for the core samples of the WD-2-1 drill hole was performed by an Analytical Spectral Device, Inc. (ASD hereafter) labspec® 5100 spec-

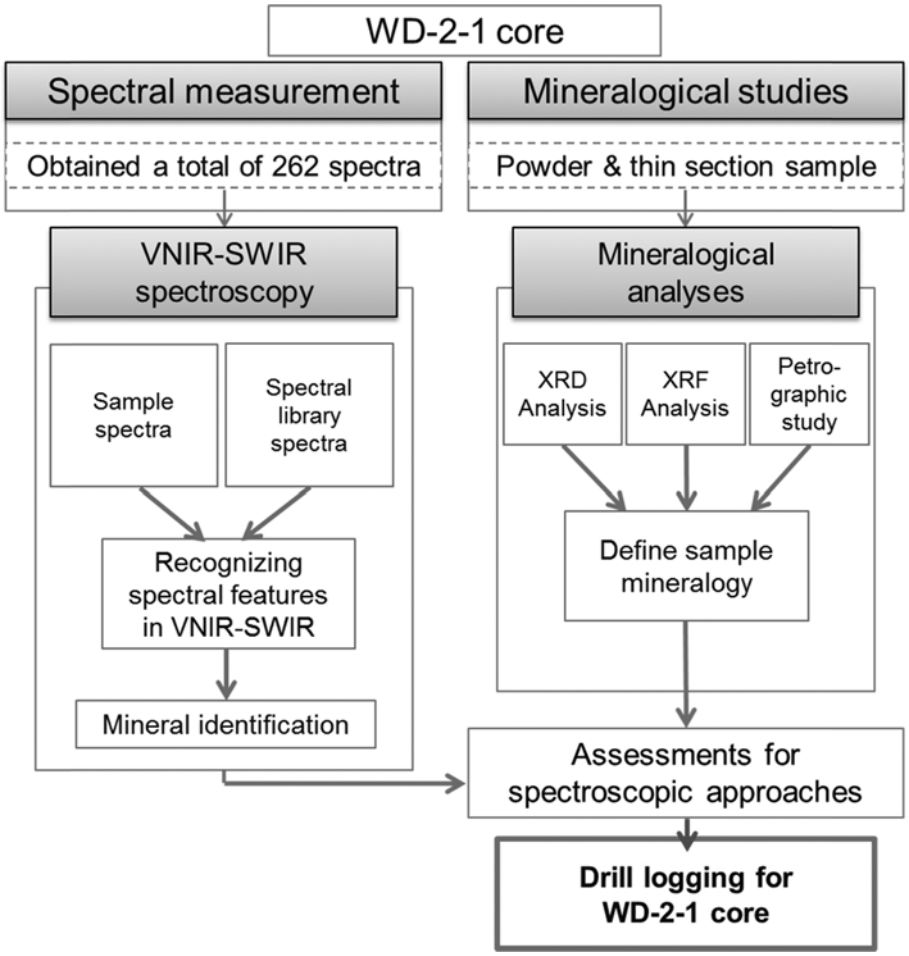

Fig. 2. Methodological procedures conducted for this study.

trometer in laboratory conditions. This instrument records the reflectance spectrum through a spectral range of 350 to 2500 nm (VNIR-SWIR region) with 3 to 6 nm of spectral resolution, which can be measured by external light-probe (for rock surface) and mug-light (for powder sample) accessories having an acquisition window of 2 cm in a spot diameter. A total of 262 spectra were obtained for the core samples of the WD-2-1 drill hole based on the light-probe mode at spacing of 1–5 m. A more detail observation as dense as 0.1-m intervals was conducted for the samples showing variations in mineral assemblages. Furthermore, powder sample analyses had been performed for the representative samples for a comparison with other forms of analysis, such as XRD, XRF, and petrographic. RS³ and Indico Pro 6.0.6 spectrum acquisition software of ASD were used for spectra acquisition, and the Spectral Geologist 7.5 (TSG hereafter) and ENVI 4.8® (ENVI hereafter) software were utilized for spectral analysis, spectral processing, and mineral identification from the unknown spectra. This study utilized United Stated Geological Survey (USGS hereafter) spectral library 06 (Clark et al., 2007) and Jet Propulsion Laboratory (JPL hereafter) ASTER spectral library version 2.0 (Bladridge et al., 2009) for mineral identification.

A mineral identification procedure based on spectral analysis involves a comparison of reference spectra and unknown sample spectra in terms of the wavelength position, intensity, and the shape of absorption features (Thompson et al., 1999; Kerr et al., 2011). Although an automated mineral identification can be useful to simplify the process of spectral analysis, the results must be individually interpreted by the user, as automated results cannot always provide a reliable output (Kerr et al., 2011). To minimize misinterpretation, this study first selected candidate spectra with automated process. Among the candidate minerals, the minerals showing a good fitness above 95% between reference spectra and the unknown spectra were selected for the most probable candidates by automated fitness algorithm in the TSG. This algorithm is using statistical methods which based on the normalization of reflectance scale, and it calculates similarities between unknown (sample) and reference (mineral) spectra. The result of matching value is scaled between 0 and 1 (percentage) and is a measure of a good fitness with 1 being a perfect match and 0 indicating no similarities between sample and reference spectra (Merry et al., 1999).

In addition, the selected candidate spectra were manually confirmed for both the reflectance spectrum and hull quotient spectrum modes for the final spectroscopic mineral identifications. This study followed six steps to extract mineral information from unknown sample spectra modified from Pontual et al. (2012): 1) Obtaining the representative spectrum of samples; 2) Observing absorption features at the SWIR (1300–2500 nm) region for skarn, alteration, and rock-forming mineral detection; 3) Identifying the deepest absorption features with special attention in the 2050–2450 nm showing the diagnostic absorption features of major components; 4) Finding the closest match to the reference spectrum of the spectral library in the 1300–2500 nm and 2050–2450 nm regions; 5) Examining possibilities of spectra mixtures of multiple minerals; and 6) Finalizing mineral combinations of sample spectra using VNIR characteristics as supplementary information.

In real-world cases, a sample spectrum with a mixture of various mineral spectra is commonly observed. A sample spectrum contains spectral characteristics of multiple minerals, and thus the absorption features of the coexisting minerals often overlap, causing a complication in identifying all coexisting minerals (Clark, 1999; Yang et al., 2000). In particular, the identification of most rock-forming anhydrous silicate minerals (e.g., feldspar and quartz) is troublesome, as those minerals provide relatively weak spectral characteristics compared to infrared-active minerals (Thomson et al., 1999; Hauff, 2008; Kerr et al., 2011). Therefore, a special interpretation approach is required to identity anhydrous silicate minerals if they are mixed with infrared-active minerals. This study employed a three-step interpretation method for mixed spectra. First, the infrared-active minerals were identified based on their distinctive absorption features. Then, reference spectra of minerals with weak spectral characteristics were compared with the sample spectrum in the SWIR region, and their probable candidates were narrowed down (Fig. 3). Finally, additional spectral characteristics in the VNIR region was compared with the candidate reference spectra, and the most probable mineral was identified. This method enabled the identification of both infrared-active minerals and the minerals having weak spectral characteristics such as feldspar and quartz in this study.

3.3. Mineralogy and Petrology

To assess the effectiveness of spectroscopic approaches, mineralogical analyses were conducted by XRD, XRF, and petrographic studies to verify the mineral assemblages from spectroscopic approaches. The XRD analysis data for 29 representative samples was produced by a Rigaku Smart Lab® X-ray Diffractometer (CuKα = 1.541862 Å) at KIGAM with the following conditions: 40kV, 30mA, 0.02°, intervals within the 3~60° 2θ range, and analytical timing of 4° 2θ/min. Ten major chemical compounds including SiO_2, Al_2O_3, Fe_2O_3, CaO, MgO, K_2O, Na_2O, TiO_2, MnO, and P_2O_5 were analyzed by an X-ray fluorescence spectroscopy (MXF-2400 Multi-channel Spectrometer, SHIMADZU Co., Japan) at KIGAM. The XRF measurement condition was at a spectrometer atmosphere of vacuum mode and measuring rates of 40 kV, 70 mA, and 2.8 kW using an X-Ray tube of an End-window type with an Rh target. The XRF measurement was made for 15 representative samples. Furthermore, petrographic observations of 21 samples were made.

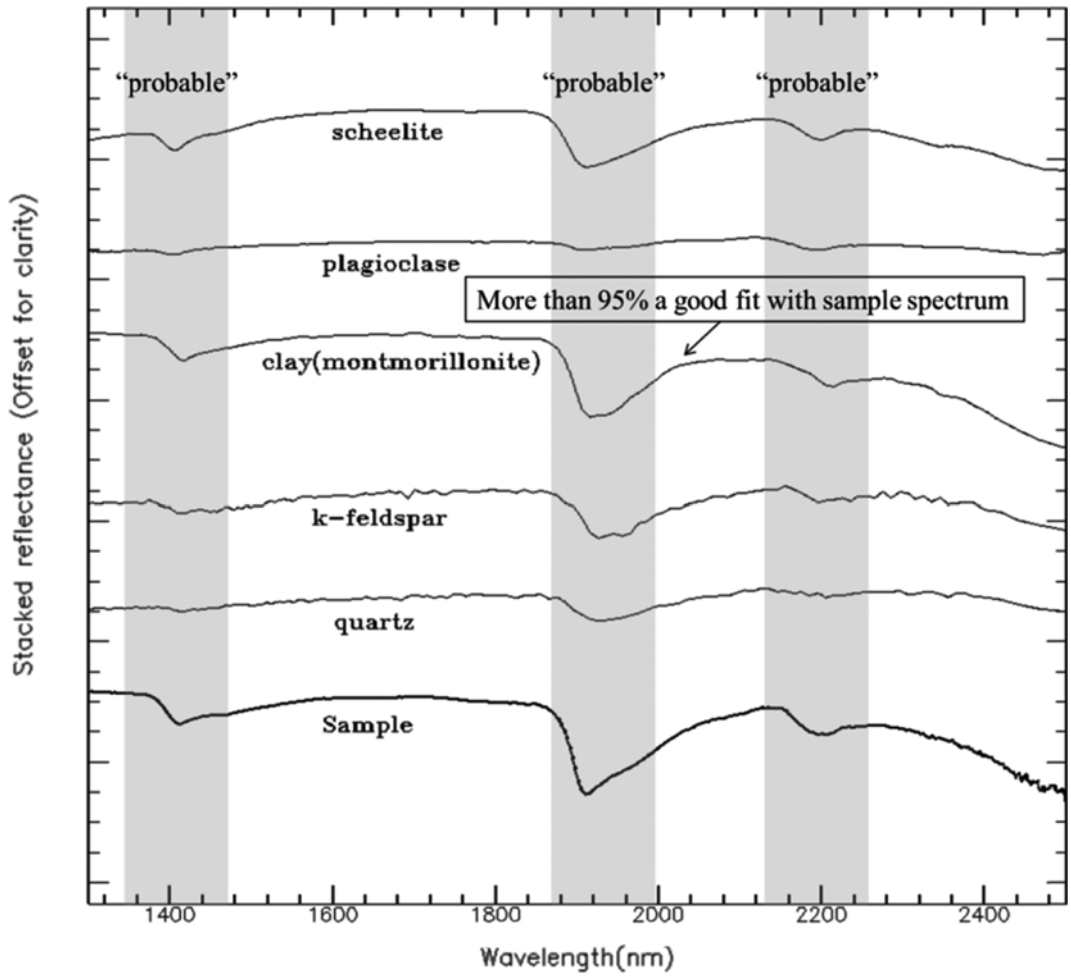

Fig. 3. Diagram showing the SWIR spectral analysis procedure in the selection of the candidate minerals based on three-step spectral checking. The infrared-active minerals (e.g., clay minerals) are easily identified based on their distinctive absorption features, and reference spectra of minerals with weak spectral characteristics compared with the sample spectrum in SWIR region could be selected as a probable candidate.

4. RESULTS AND DISCUSSION

4.1. Spectral Characteristics of the Core Samples of the WD-2-1 Drill Hole

Based on the VNIR-SWIR spectroscopic analyses of 262 spectra, the spectral characteristics of WD-2-1 were defined. The spectroscopy revealed that the core samples include intrusive rock, host rock, two different types of skarn, and W-ore zones. The intrusive rock mainly consisted of quartz porphyry occupying a 0–123 m section of the core. The spectroscopy identified K-feldspar, plagioclase, and quartz and clay minerals, and secondary minerals such as calcite, chlorite, clinopyroxene, fluorite, garnet, scheelite, and vesuvianite were observed locally in the intrusive rock section (Table 2). Following the intrusive rock, two types of skarn zones were recognized. The skarn zones were classified into garnet-clinopyroxene and clinopyroxene-garnet based on the frequency of sample spectra. The garnet-clinopyroxene skarn zone was located at 123–240 m of the core, and spectra of calcite, chlorite, clays, clinopyroxene, fluorite, K-feldspar, plagioclase, quartz, scheelite, and vesuvianite mixed with garnet were observed (Table 2). Furthermore, the clinopyroxene spectrum was also mixed with the mineral spectra listed above occasionally. In the clinopyroxene-garnet skarn zone, clinopyroxene was the dominant mineral spectrum assembling with calcite, chlorite, clays, fluorite, garnet, quartz, scheelite, vesuvianite, and wollastonite spectra (Table 2). The clinopyroxene-garnet occupied a 240–307 m section of the core. The Maggol Limestone, the host rock of this ore deposit, was found in a 307–400 m section of the core, where spectra of calcite, chlorite, clays, clinopyroxene, and serpentine were detected. The W-ore zone overlapped with the intrusive rock, garnet-clinopyroxene skarn, and clinopyroxene-garnet skarn zones through a 0–307 m section (Table 2).

Table 1. The common absorption features of major components in the SWIR region (combined from Hauff, 2008; Herrmann et al., 2001; Pontual et al., 2012)

Absorption feature position (nm)	Major component	Mineral group
~1400 and ~1800	OH	Clays, hydroxides, zeolites
~1400 and ~1900	H_2O	Clays
2160–2228 (weaker at 2340–2440 by 2nd Al-OH)	Al-OH	Clays, K-micas
2230–2298 and ~2350	Fe-OH	Fe-clays, chlorite
2300–2360	Mg-OH	Mg-clays, chlorite
2300–2350 (and also at 1870, 1990, 2155)	CO_3	Carbonates

Table 2. Identified mineral information based on the reflectance spectroscopy, XRD analysis, and petrographic study from the samples

Zonation	Depth (m)	Reflectance spectroscopy		XRD analysis		Petrographic study	
		Number of measurement	Minerals	Number of measurement	Minerals	Number of measurement	Minerals
Intrusive rock (contains W-ore zone)	0–123	54	Cal, Chl, Clays, Cpx, Fl, Grt, Kfs, Pl, Sch, Ves, Qz,	9	Cal, Chl, Clays, Cpx, Fl, Grt, Kfs, Ms, Pl, Sch, Ves, Qz, Zeo	3	Cal, Clays, Cpx, Kfs, Ser, Ves, Qz
Grt-cpx skarn zone (contains W-ore zone)	123–240	69	Cal, Chl, Clays, Cpx, Fl, Grt, Kfs, Pl, Sch, Scp, Ves, Wo, Qz	10	Cal, Chl, Clays, Cpx, Grt, Kfs, Sch, Scp, Ves, Wo, Qz	8	Cal, Clays, Cpx, Grt, Scp, Ser, Ves, Wo, Qz
Cpx-grt skarn zone (contains W-ore zone)	240–307	91	Cal, Chl, Clays, Cpx, Fl, Grt, Sch, Ves, Wo	6	Cal, Chl, Cpx, Grt, Kfs, Ves, Wo, Qz	6	Cal, Cpx, Clays, Grt, Kfs, Ves, Wo, Qz
Host rock	307–400	48	Cal, Chl, Clays, Cpx, Srp	4	Cal, clays, Cpx, Kfs, Qz	4	Cal, Chl, Clays, Cpx, Qz

In this study, clays include representative clay minerals such as illite, kaolinite, and montmorillonite.
Abbreviations (after Whitney and Evans, 2010): Cal = calcite; Chl = chlorite; Cpx = clinopyroxene; Fl = fluorite; Grt = garnet; Kfs = K-feldspar; Ms = muscovite; Pl = plagioclase; Sch = scheelite; Scp = scapolite; Ser = sericite; Srp = Serpentine; Ves = vesuvianite; Wo = wollastonite; Qz = quartz; Zeo = zeolite.

4.1.1. Representative spectral characteristics of intrusive rock

The representative sample, WD-1, of major rock-forming minerals in the intrusive rock zone included clays, K-feldspar, plagioclase, and quartz; the sample spectrum contained absorption features at 600 nm, 960 nm, 1350 nm, 1400 nm, 1450 nm, 1900 nm, 2100 nm, 2200 nm, 2350 nm, and 2450 nm. The most obvious absorption features around 1400 nm and 1900 nm were caused by OH and H_2O, and 2200 nm absorption was diagnostic absorption features caused by Al-OH (Fig. 4a, Table 1) (Herrmann et al., 2001; Hauff, 2008; Pontual et al., 2012). In the VNIR region, the spectrum showed a similar broaden absorption feature of plagioclase at 600 nm, and keen absorption at 960 nm by clays (illite) + quartz (Fig. 4a). Furthermore, in the SWIR region, the spectral shoulders around 1350 nm and 1450 nm caused by clays (illite) + quartz were also observed. Absorption features in the SWIR region including 1400 nm, 1900 nm, 2100 nm, 2200 nm, 2350 nm, and 2450 nm were affected by clays (illite) + quartz, K-feldspar and plagioclase (Fig. 4a).

The representative calcite veinlet sample in the intrusive rock, WD-2 sample, showed a spectral characteristics of calcite, clays (montmorillonite), and vesuvianite identified by absorption features around 950 nm, 1100 nm, 1450 nm, 1900 nm, 2000 nm, 2200 nm, and 2350 nm (Fig. 4b). The absorption feature around 900 nm and broaden absorption feature around 1100 nm were known to be caused by Fe components (Pontual et al., 2012) where those absorptions were caused by vesuvianite in the sample (Fig. 4b). The doublet around 1450 nm coincided well with that of vesuvianite (Fig. 4b). Moreover, absorption features in the SWIR region, 1900 nm, 2000 nm, 2200 nm, and 2350 nm, indicated that the spectral curve was affected by both calcite + clay (montmorillonite) and vesuvianite where the absorption feature at 2350 nm was the diagnostic absorption of the CO_3 of calcite and the Mg-OH/Al-OH of vesuvianite (Fig. 4b, Table 1) (Herrmann et al., 2001; Pontual et al., 2012).

The two types of skarn veinlets identified by spectral analysis were clinopyroxene and fluorite-chlorite veinlets. The spectrum of the clinipyroxene veinlet, WD-3, contained spectral information of clinopyroxene, K-feldspar, and plagioclase where broaden absorption features around 700–800 nm and 1100–1200 nm were caused by ferrous features of clinopyroxene (Hauff, 2008; Pontual el al., 2012). The absorption features around 1400 nm, 1900 nm, 2200 nm, and 2350 nm

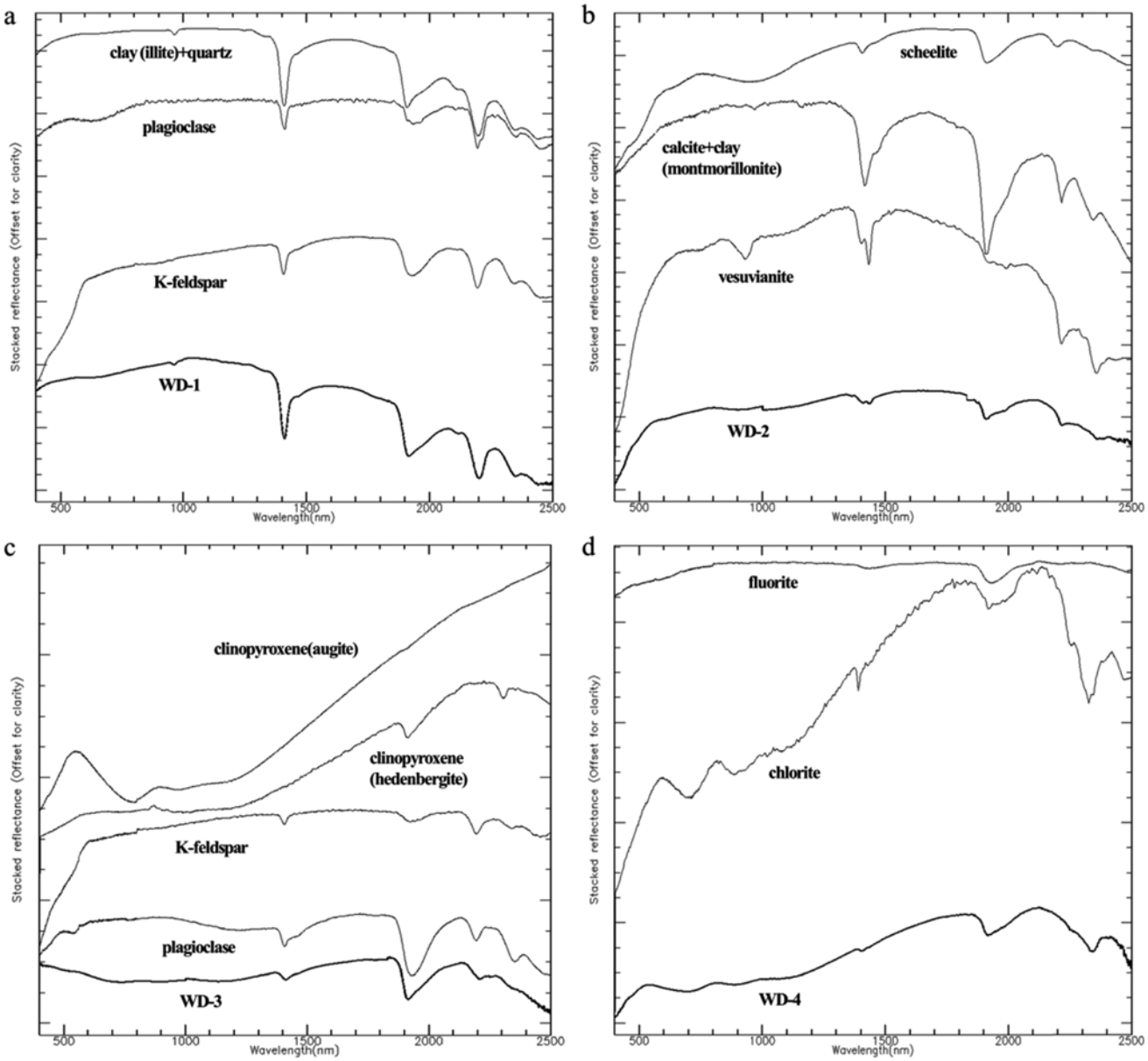

Fig. 4. Representative sample reflectance spectra (WD-1, WD-2, WD-3, and WD-4) overlaid with reference spectra in the intrusive rock zone; (a) Reflectance spectrum of the WD-1 sample compared to the reference spectra of clay (illite) + quartz, K-feldspar, and plagioclase, (b) The reflectance spectrum of the WD-2 sample overlaid with the reference spectra of calcite + clay (montmorillonite), scheelite, and vesuvianite mixtures, (c) The reflectance spectrum of the WD-3 sample matched with the reference spectra of clinopyroxene (hedenbergite, augite), K-feldspar, and plagioclase, and (d) The reflectance spectrum of the WD-4 sample with the reference spectra of chlorite and fluorite.

were affected by K-feldspar and plagioclase (Fig. 4c). The fluorite-chlorite veinlet sample, WD-4, imprinted the absorption features of chlorite around 700 nm, 900 nm, and a broaden absorption around 1150–1250 nm caused by the Fe component of chlorite where those diagnostic features helped in the detection of chlorite in the VNIR range due to relatively less interference (Hauff, 2008). Moreover, the absorption features in SWIR included chlorite absorptions around 1400 nm and 1900 nm, and diagnostic absorptions of 2250 nm and 2350 nm while 1900 nm absorption also indicated that of fluorite (Fig. 4d, Table 1) (Herrmann et al., 2001; Hauff, 2008; Pontual et al., 2012).

4.1.2. Representative spectral characteristics of the garnet-clinopyroxene skarn zone

Clay (montmorillonite), garnet (grossular), and vesuvianite spectral features were presented in the spectrum of WD-5 (Fig. 5a). Garnet is considered to be a main indicator of skarn alterations, as VNIR spectral characteristics were well recognized at absorption around 450 nm and 950 nm, and at

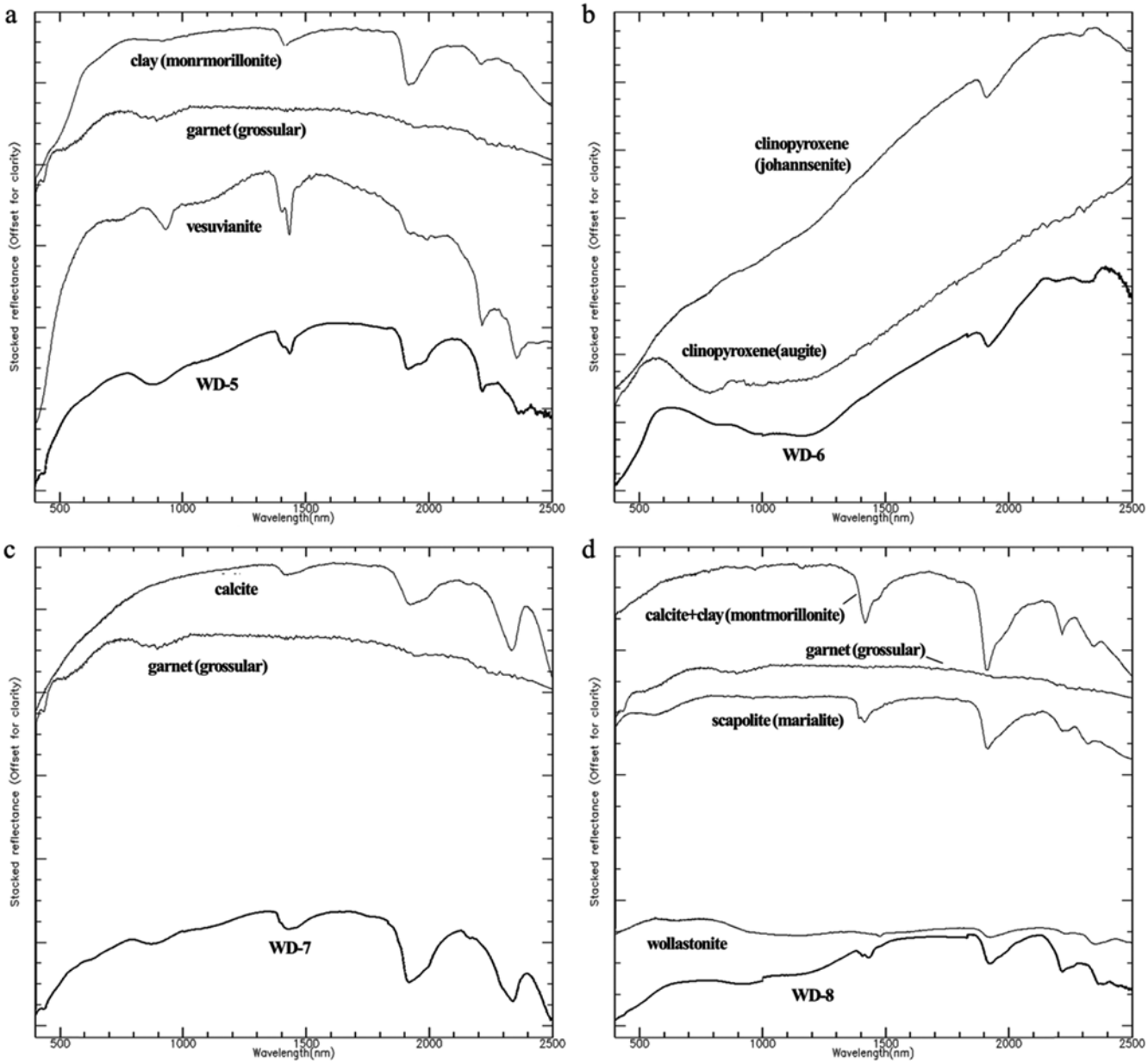

Fig. 5. Representative sample spectra of the garnet-clinopyroxene skarn zone (WD-5, WD-6, WD-7, and WD-8) referenced to standard spectra of major skarn and clay minerals; (a) Reference spectra of clay (montmorillonite), garnet (grossular), and vesuvianite and WD-5 spectrum, (b) The WD-6 reflectance spectrum and clinopyroxene (augite and johannsenite) reference spectra, (c) The WD-7 spectrum overlaid with the reference spectra of calcite and garnet (grossular), and (d) The WD-6 spectrum and the reference spectra of calcite + clay (montmorillonite), garnet (grossular), scapolite (marialite), and wollastonite.

spectral shoulder near 600 nm (Hauff, 2008). In addition, absorption features of vesuvianite such as 1400 nm doublet and absorptions around 2200 nm and 2350 nm were observed while the spectral curve at the SWIR region 1900–2000 nm overlapped well with both montmorillonite and vesuvianite (Fig. 5a, Table 1).

Two different types of clinopyroxene were spectrally observed from the WD-6 sample (Fig. 5b). Clinopyroxene is believed to be one of the main indicators of skarn mineralization along with garnet where diagnostic spectral features can be observed in the NIR region (Hauff, 2008). The spectral curve of WD-6 showed a similar pattern to that of augite in the 800–1200 nm range, and the reflectance increased from 1200 nm to 2500 nm where it coincided well with both augite and johannsenite (Fig. 5b). Moreover, the diagnostic absorptions of johannsenite around 1900 nm and 2300 nm were observed (Fig. 5b).

The spectrum of the WD-7 sample suggested the existence of calcite and garnet in the garnet-clinopyoxene zone where the spectrum overlapped with garnet in the VNIR region

and with calcite in the SWIR region, showing almost identical shapes and intensities of absorption features (Fig. 5c). Finally, calcite, clay (montmorillonite), garnet, scapolite (marialite), and wollastonite were spectrally detected from the WD-8 sample (Fig. 5d). It also illustrated garnet's spectral pattern in VNIR, whereas spectral characteristics of calcite + clay (montmorillonite), scapolite, and wollastonite were observed in the SWIR region. The existence of scapolite was confirmed by doublet features around 1400 nm, and calcite + clay (montmorillonite) was involved with absorptions around 1900 nm and 2200 nm, which also overlapped with scapolite. Wollastonite's spectral feature includes absorption around 1350 nm and a flat spectrum around 500 nm (Fig. 5d).

4.1.3. Representative spectral characteristics of the clinopyroxene-garnet skarn zone

In this section, a sole spectrum of clinopyroxene is observed in many cases such as the spectral curve of the WD-9 sample (Fig. 6a). Garnets occurring this zone often displayed a spectral mixture with calcite such as the spectrum of WD-10 (Fig. 6b). The spectral curve of WD-10 showed garnet's spectral feature in the VNIR region, and spectral features of calcite matched well in the SWIR region (Fig. 6b).

4.1.4. Representative spectral characteristics of host rock

The sole spectrum of calcite is the most dominant spectrum observed in the host rock section such as that of WD-11, showing a perfect match of absorption features with calcites in the SWIR region (Fig. 7a). In addition to the sole spectrum of calcite, the spectral mixture of calcite and chlorite was observed locally, as the spectral curve of WD-12 shows. The absorption features caused by the Fe component of chlorite were observed around 600 nm, 900 nm, and 1200 nm whereas absorption features in the SWIR region overlapped with both calcite and chlorite (Fig. 7b). Furthermore, a mixed spectrum of serpentine and calcite was observed. The mixed spectrum (WD-13) included absorption features at 450 nm, 670 nm, 1100 nm, 1390 nm, 1950 nm, and 2340 nm corresponding with serpentine. In particular, the distinctive absorptions of serpentine were detected around 450 nm and 1390 nm, and overlapping absorptions of calcite and serpentine appeared at 1950 nm and 2340 nm (Fig. 7c).

4.1.5. Representative spectral characteristics of the W-ore zone

The spectral features of scheelite include a wide absorption around 950 nm and additional absorptions at 1400 nm, 1900 nm, and 2200 nm. WD-14 ideally matched with the reference curve (Fig. 7d).

4.2. Assessment of Spectroscopic Analysis

The mineral combination for each zone including intrusive, two types of skarn, and host rock identified from spectroscopic analysis were cross-validated with XRD and petrographic analyses (Table 2). In general, the agreement between the spectroscopy and XRD and petrographic studies was tested. However, the existence of fluorite, plagioclase, and scheelite was only confirmed in the intrusive rock from XRD and petrographic studies, whereas a discrepancy occurred in skarn zones in general (Table 2). Moreover, the serpentine spectrum distinctively identified in host rock does not match with XRD and petrographic analyses (Table 2). In general, the mineral composition of the intrusive rock (quartz porphyry)

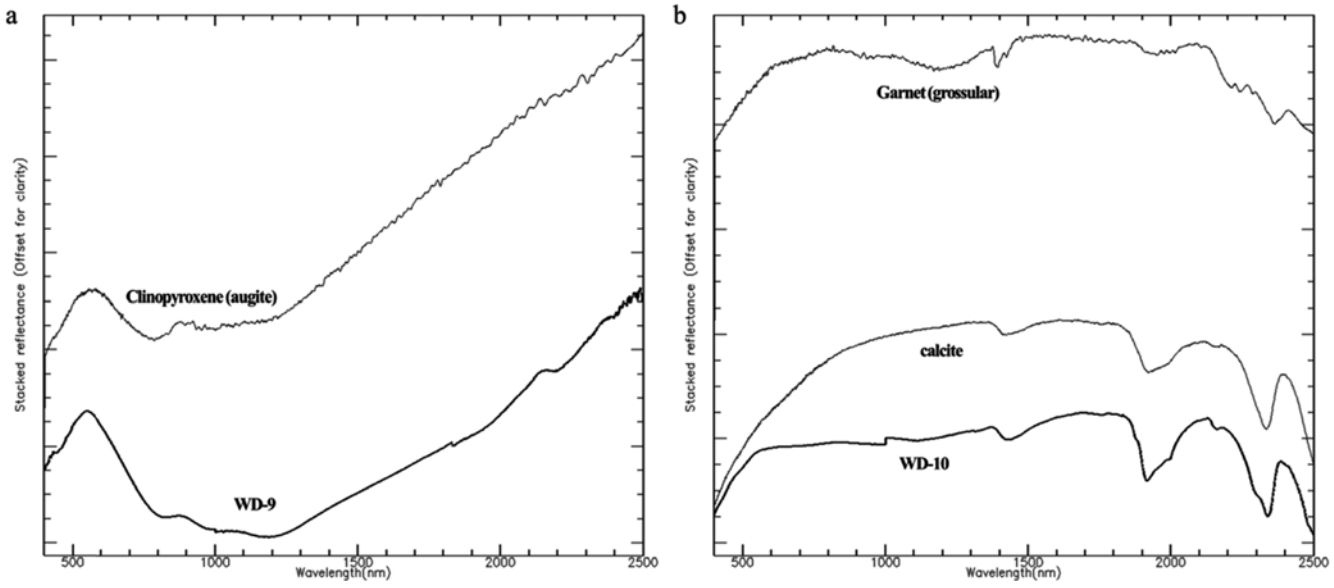

Fig. 6. Representative sample spectra of the clinopyroxene-garnet skarn zone overlaid with the reference spectral of calcite, clinopyroxene, and garnet by spectral similarity; (a) The WD-9 sample spectrum corresponding with clinopyroxene (augite) reference and (b) The WD-10 sample spectrum compared to the reference spectra of calcite and garnet (grossular).

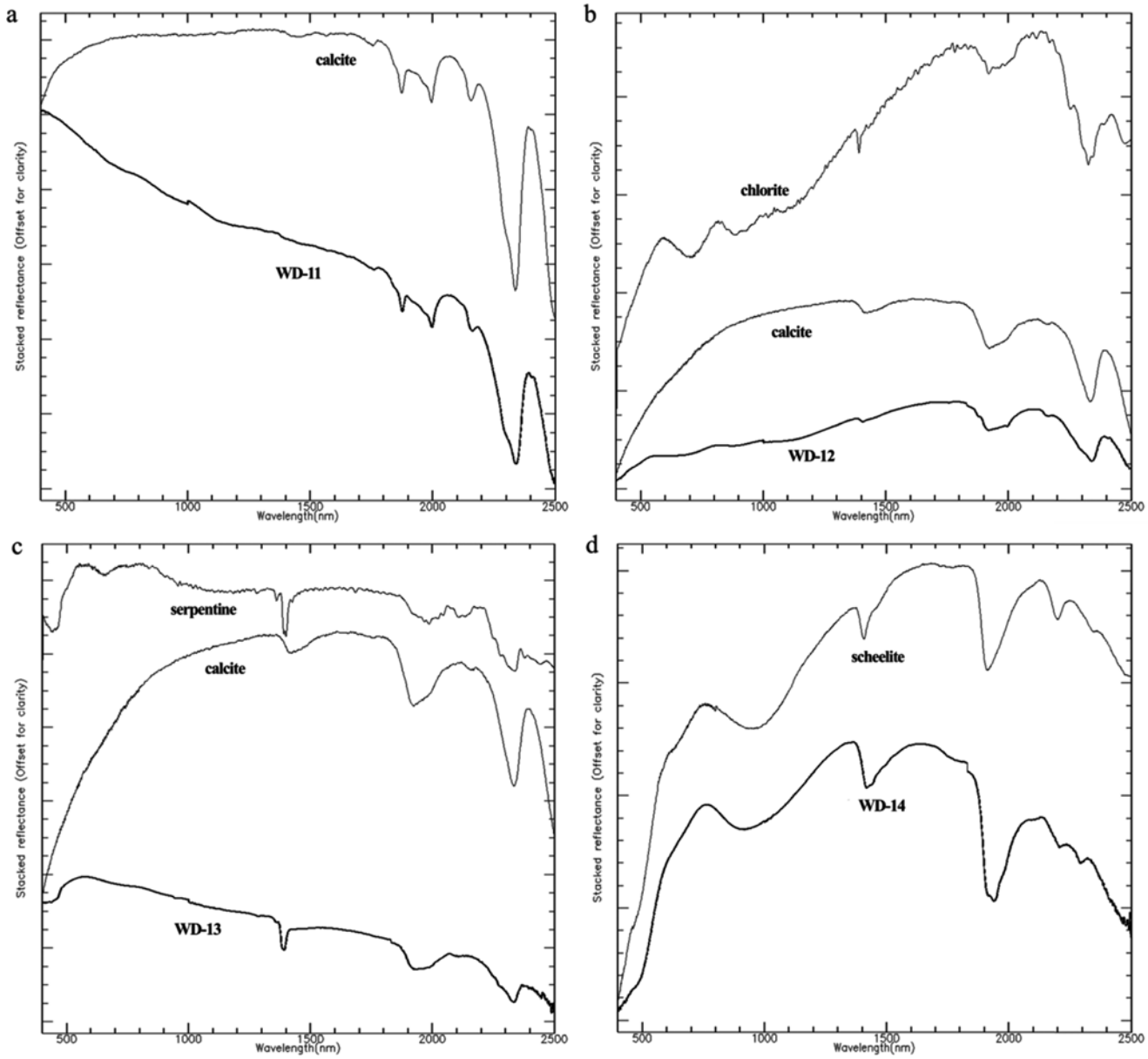

Fig. 7. Representative sample spectra of the host rock (a–c) and W-ore zones (d) matched with the reference spectra of calcite, chlorite, serpentine, and scheelite; (a) The WD-11 spectrum showing the diagnostic absorption features of calcite, (b) The WD-12 reflectance spectrum showing spectral features matching with calcite and chlorite reference spectra, (c) The spectrum of WD-13 sample matched with the reference spectra of calcite and serpentine, and (d) the spectrum of the WD-14 sample representing W mineralization matched with the scheelite reference spectrum.

did not involve infrared-active minerals except clays, as quartz porphyry mostly consists of anhydrous silicate minerals. This mineral composition eased the extraction of spectral characteristics of fluorite, plagioclase, and scheelite because the spectral disruption by other minerals was relatively minimal. However, skarn minerals are mostly infrared-active minerals with distinctive absorption features, and thus the spectral features of fluorite, plagioclase, and scheelite are often confused. It can be inferred that spectroscopic analysis for fluorite, plagioclase, and scheelite in skarn zones is relatively uncertain.

On the other hand, the existence of K-feldspar and quartz in the intrusive rock and garnet-clinopyroxene skarn zones corresponded with XRD and petrographic analyses, despite the indistinctive spectral features. However, K-feldspar and quartz showed disagreement in the clinopyroxene-garnet and host rock zones. We suspect that this phenomenon was closely related to the abundance of mineral composition. Thomson et al. (1999) reported that the dominant reflective mineral with 10% or more can be easily founded in the sample spectrum whereas minerals less than 5% induce uncertainty in the spectrum. It should be noted that although this

study identified the most rock-forming anhydrous silicate minerals including quartz, K-feldspar, and plagioclase, it doesn't mean that they are always identifiable. Thus, it would be better approach to incorporate additional mineral identification tools for those minerals. Indeed, anhydrous silicate minerals are known to have the diagnostic spectral characteristics in thermal infrared region (TIR hereafter) (Ninomiya and Fu, 2002; Ninomiya, 2002; Ninomiya, 2003a and 2003b; Rowan and Mars, 2003; Ninomiya and Fu, 2010; Corrie et al., 2011; Ninomiya et al., 2005; Aboelkhair et al., 2010; Son et al., 2014). Therefore, if TIR studies were attached in this study, the certainty could be increased to recognize the anhydrous silicate minerals.

The petrographic observation confirmed that K-feldspar and quartz were clearly the major minerals in the intrusive rock and garnet-clinopyroxene skarn zones whereas their occurrence was minor in the clinopyroxene-garnet skarn and host rock zones (Fig. 8). Moreover, fluorite, plagioclase, and scheelite were rarely observed in the photomicrograph of intrusive rock and skarn zones, which also confirmed the relationship between mineral abundance and the certainty of spectroscopic analysis.

Furthermore, muscovite and zeolite were detected by XRD analysis where spectroscopy failed to detect in the intrusive rock zone (Table 2). Their spectral features overlap with clay minerals, which were dominantly observed in all sections. As Figure 9 shows, the absorption features of muscovite are identical with clay-a whereas those of zeolite is the same as clay-b, except the absorption of clay-b at 2200 nm. This suggests that if clay minerals are dominant, muscovite and zeolite are impossible to distinguish based on spectroscopic approaches. Sericite (fine-grained K-micas) was observed in intrusive rock and garnet-clinopyroxene zones under petrographic study while spectroscopy failed due to the tiny quantity (Table 2, Figs. 8a and e). In general, sericite contains the sharp Al-OH absorption feature between 2180 and 2228 nm and weaker Al-OH absorption features near 2340–2440 nm (Herrmann et al., 2001; Hinchey, 2011). They are commonly associated with hydrothermal alterations with distinctive quantities. This concludes that sericite can be spectroscopically detectable in hydrothermal mineralization while its existence in skarn mineralization involves a certain level of uncertainty due to the mineral abundance.

Skarn minerals such as calcite, chlorite, clinopyroxene, garnet, scapolite, vesuvianite, and wollastonite showed general agreement with XRD and petrographic studies (Table 2). As previously mentioned, their spectral curves were commonly in a mixture form closely related to their occurrence as skarn mineral combinations. Their spectral curves mainly involved either or both clinopyroxene and garnet, which were the major skarn minerals in the study area. The spectra mixture containing garnet commonly showed the spectra combination of garnet ± calcite ± clays ± scapolite ± vesuvianite ± wollastonite (Figs. 4c, 5a–d, 6a and b), and the spectral information of clinopyroxene could be extracted from either the single clinopyroxene spectrum or the spectra combination of clinopyroxene ± K-feldspar ± plagioclase (Figs. 4c, 5b, and 6a). Although garnet and clinopyroxene often coexisted at all of the skarn zones, no spectra had been detected containing spectral features of both (Table 2). This phenomenon can be explained by their occurrence pattern. The petrographic studies revealed that garnet and clinopyroxene coexist in many cases while their dominance varies. When garnet is dominant, clinopyroxene occurs as a diminutive quantity in forms of microcrystalline or euhedral crystals (Fig. 8e). On the other hand, garnet is rarely observed when clinopyroxene occurs dominantly (Fig. 8d). Because the spectral characteristics of garnet and clinopyroxene are completely different in the NIR region, their dominance controls the sample spectrum. On the other words, if garnet is dominant, the garnet spectrum rules out clinopyroxene spectral features and the reverse is also possible. This suggests that their coexistence cannot be easily detected with spectroscopic approaches for skarn exploration.

Conclusively, fluorite, K-feldspar, plagioclase, quartz, and scheelite did not correspond with each of zones. However, skarn minerals such as calcite, chlorite, clinopyroxene, garnet, scapolite, vesuvianite, and wollastonite showed general agreement with XRD and petrographic studies. Clay minerals also have showed well coincidence with all of zones. Furthermore, muscovite and zeolite were failed to be detected in spectroscopy because of the overlap with clay minerals. Serpentine did not match with cross-validation results (Table 2). Representatively, fluorite, K-feldspar, plagioclase, quartz, and scheelite could lead to the spectral confusion, because they have relatively weak spectral features. In particular, anhydrous silicate minerals such as K-feldspar and quartz should be accompanied with TIR analysis for the spectral certainty. The clinopyroxene and garnet well corresponded with skarn zones because of abundance effects, but they should be dealt with additional steps of spectral analysis, because they also have relatively weak spectral characteristics compared to infrared-active minerals.

4.3. Skarn Mineralization from the Core Logging of WD-2-1

The combined analyses of the spectroscopic approach, XRD analysis, and petrographic observations revealed that the skarn mineralization of the Weondong deposit is subdivided into intrusive rock, garnet-clinopyroxene skarn, clinopyroxene-garnet skarn, and host rock zones from the top to the bottom of the core. And the W-ore mineralization zone mainly overlaps with intrusive rock and garnet-clinopyroxene skarn zones (Fig. 10).

To crosscheck the drill log results and to monitor changes in chemical composition, XRF analyses were carried out. A total of 15 samples representing each zonation were analyzed and 6 chemical compounds, SiO_2, CaO, Al_2O_3, Fe_2O_3,

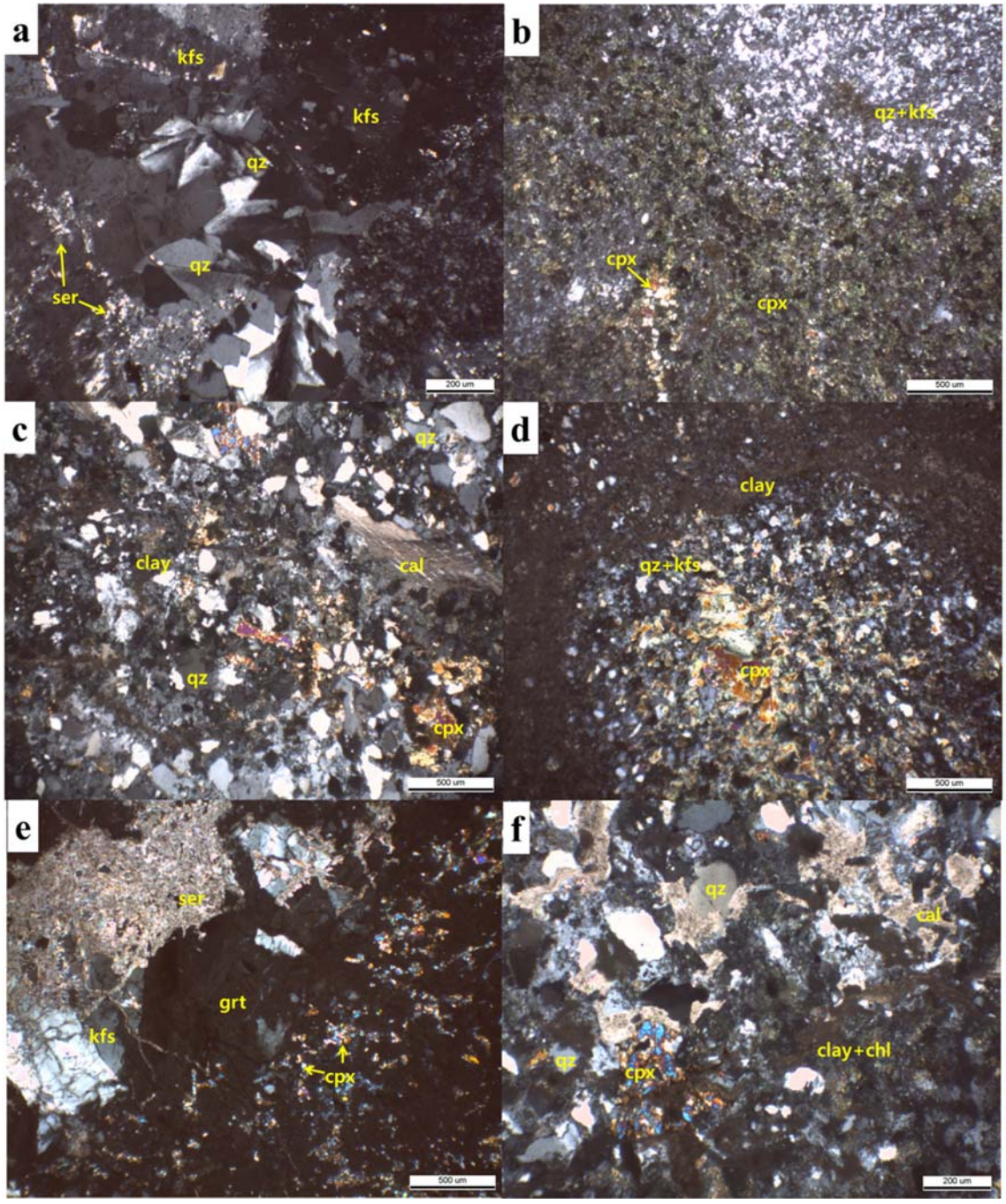

Fig. 8. Photomicrographs (crossed nicols) of representative samples showing mineral compositions for intrusive (a and b), garnet-clinopyroxene (c and e), clinopyroxene-garnet zones (d), and host rock (f); (a and b) mineral assemblages of clinopyroxene, K-feldspar, quartz, and sericite in the intrusive rock zone, (c and e) the major abundance of K-feldspar, garnet and quartz with calcite, clay, clinopyroxene, and sericite at the garnet-clinopyroxene skarn zone, (d) the major abundance of clinopyroxene coexisting with clay, K-feldspar, and quartz in the clinopyroene-garnet skarn zone, (f) the mineral assemblage of calcite, chlorite, clinopyroxene, and minor quart in the host rock zone (Abbreviations after Whitnet and Evans, 2010).

K_2O, and MgO, closely related to the mineralization were drawn over the drill log for better comparison (Fig. 10). The SiO_2 content, which is the main chemical component of all silicate minerals, well correlated with zone definition, showing a higher content at the top of the core with a decreasing trend as the depth increased with a range of 45–75 wt%. It can be inferred that the chemical reaction between the intrusive rock and the host rock related to skarn mineralization increased downward and eventually converted to the garnet-clinopyroxene zone. The same trend was also observed

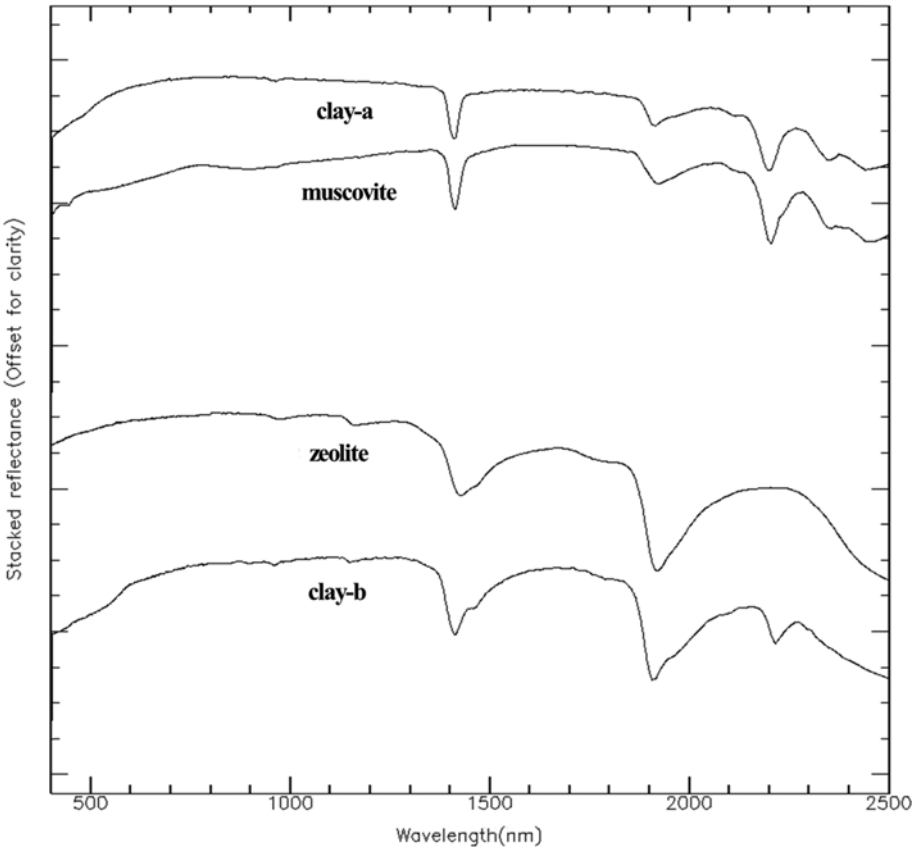

Fig. 9. Spectral similarities of clay minerals, zeolite, and muscovite leading to complications in mineral identification.

with Al_2O_3 and K_2O, indicating the depletion of rock forming minerals such as quartz, plagioclase, and K-feldspar downward as skarn mineralization increased. This result identically matched with the mineral combination and zonation defined by spectroscopic approaches (Fig. 10). On the other hand, the inverse correlation of CaO content to SiO_2 content was well presented, showing an increasing trend (Fig. 10). This strongly suggested the participation of carbonate minerals in the skarn mineralization between the intrusive and the host rocks.

The chemical compositions of SiO_2, CaO, Al_2O_3, Fe_2O_3, and MgO fluctuated significantly with irregular patterns in the skarn zones whereas the K_2O content was constantly depleted. This phenomenon indicates that the intensity of a metasomatic reaction between intrusive and the carbonate host rocks varies significantly, which is closely related to skarn mineralization. Moreover, the depletion of K_2O infers

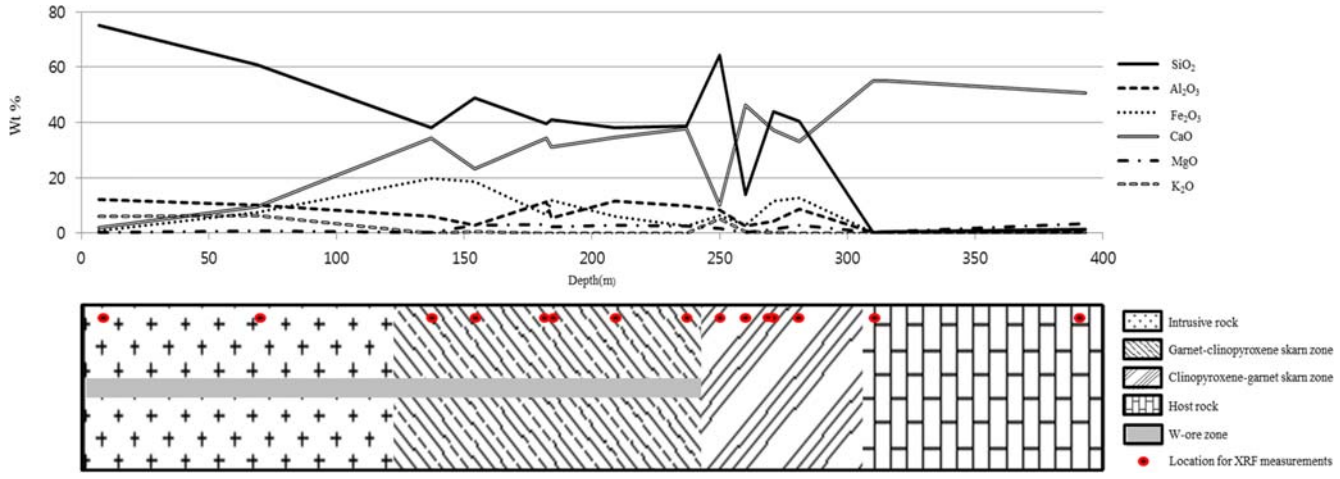

Fig. 10. The core logging of the WD-2-1 drill hole based on the spectroscopic analyses is subdivided into intrusive rock, garnet-clinopyroxene skarn, clinopyroxene-garnet skarn, host rock, and W-ore zones by mineral assemblages following the spectral frequency. A total of 15 samples for XRF analysis show the trend of SiO_2, CaO, Al_2O_3, Fe_2O_3, K_2O, and MgO contents.

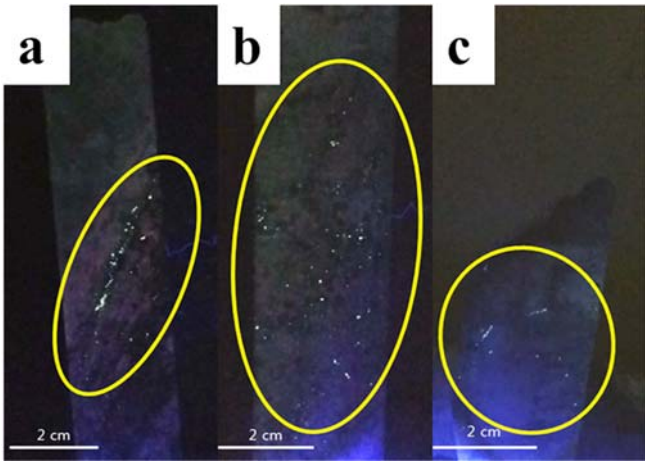

Fig. 11. Occurrences of W-minerals in the veinlet (a), and disseminated grains (b and c) detected under UV short fluorescence in the intrusive rock (a and b) and garnet-clinopyroxene skarn (c) zones.

the depletion of K-feldspars and the richness of skarn minerals in the skarn zones. However, the XRF results could not be crosschecked with specific mineral combinations defined by spectroscopic approaches while the definition of skarn zones induced from spectroscopy corresponds well with the XRF results (Fig. 10).

W mineralization had been confirmed by spectroscopy and XRD analyses overlapping with the intrusive rock and garnet-clinopyroxene skarn zones (Table 2). Because XRF does not detect W mineralization, the existence of the scheelite was double-checked with UV lamp scanning. The results confirmed that disseminated scheelite crystals distributed with the skarn minerals in the intrusive rock and garnet-clinopyroxene skarn zones (Fig. 11). This indicates that the ore mineralization had been more active in the intrusive rock side and the contact between the intrusive rock and skarn zones while ore mineralization was diminished in the host rock ward.

In general, the skarn zonation from the intrusive rock is defined as proximal endoskarn to proximal exoskarn, indicated by the dominance of garnet. As the distance from the intrusive body increases, the distal skarn is more dominated by pyroxene specifically near the contact point with carbonate host rocks (Meinert et al., 2005). Our study for the core samples of the WD-2-1 drill hole correlated well with the definition of skarn zonation where the W mineralization in the study area mainly occurred along the proximal endoskarn and exoskarn while the distal skarn zone was lacking W mineralization. In conclusion, the spectroscopic approaches are effective for identifying skarn zonation and mineralization. It is expected that the spectroscopic approach in skarn exploration would provide a great convenience with a certainty.

5. CONCLUSIONS

This study examined the spectral characteristics of minerals occurring at Weondong skarn deposit and assessed the effectiveness of VNIR-SWIR spectroscopic approaches in zone definition characterizing skarn deposits based on XRD, XRF, UV lamp scanning, and petrographic studies. The spectroscopic analyses identified intrusive rock, garnet-clinopyroxene skarn, clinopyroxene-garnet skarn, W-ore, and host rock zones for the cores of the WD-2-1 drill hole. The spectrometry could provide mineral assemblages corresponded with each zone. The intrusive rock zone mainly consisted of clay minerals, K-feldspar, plagioclase, and quartz and accessary minerals including calcite, chlorite, clinopyroxene, fluorite, garnet, scheelite, and vesuvianite. The garnet-clinopyroxene and clinopyroxene-garnet skarn zones were defined by the frequency of clinopyroxene or garnet spectra. The two types of skarn zones mainly consisted of calcite, chlorite, clays, clinopyroxene, fluorite, garnet, K-feldspar, plagioclase, quartz, scapolite, scheelite, vesuvianite, and wollastonite. The host rock zone mainly consisted of calcite, chlorite, clays, clinopyroxene, and serpentine. The assessment results for VNIR-SWIR spectroscopy in skarn exploration illustrated that the spectral approaches would be useful for attaining skarn mineral information such as calcite, chlorite, clinopyroxene, garnet, scapolite, vesuvianite, and wollastonite and clay minerals. However, the minerals such as clinopyroxene and garnet with relatively weak spectral characteristics may require additional analytical steps for the spectral certainty in mixture status. Furthermore, the rock-forming minerals such as fluorite, K-feldspar, plagioclase, quartz, sericite, and scheelite did not always correspond with all zones due to the relationship of infrared-active mineral effects or mineral abundance. The zonation of the study core constructed by combined analyses of spectrometry, XRD, XRF, and petrographic studies revealed that higher SiO_2, Al_2O_3, and K_2O contents' components correlated well with the zone of intrusive rock and decreasing content trends of those components as the depth increased, indicating the transition from intrusive rock to skarn mineralization. On the other hand, the CaO content was inversely correlated with SiO_2, thus showing the participation of carbonate minerals in the skarn mineralization between the intrusive rock and the host rock. Moreover, the chemical compositions of SiO_2, CaO, Al_2O_3, Fe_2O_3, and MgO fluctuate substantially with an irregular pattern. This suggests that the intensity of a metasomatic reaction between intrusive rock and the carbonate host rocks varies significantly by location. Besides, the depletion of K_2O inferred the depletion of K-feldspars and the richness of skarn minerals in the skarn zones. Moreover, W mineralization was detected in the intrusive rock and garnet-clinopyroxene skarn zones, which indicated that the ore mineralization had been more active in the intrusive rock side and their contact with skarn zones. In conclusion, the W-skarn mineralization of the study core was defined as proximal endoskarn to proximal exoskarn, which could be identified by spectroscopic approaches.

ACKNOWLEDGMENTS: This work was supported by the National Research Foundation of Korea Grant, funded by the Korean Government under Grant NRF-2012R1A1A104589.

REFERENCES

Aboelkhair, H., Ninomiya, Y., Watanabe, Y., and Sato, I., 2010, Processing and interpretation of ASTER TIR data for mapping of rare-metal-enriched albite granitoids in the Central Eastern Desert of Egypt. Journal of African Earth Sciences, 58, 141–151.

Bladridge, A.M., Hook, S.J., Grove, C.I., and Rivera, G., 2009, The ASTER spectral library version 2.0. Remote Sensing of Environment, 113, 711–715. http://speclib.jpl.nasa.gov

Chi, S.J., Kang, I.-M., Kim, Y.U., Kim, E.-J., Kim, I.J., Park, S,-W., Lee, J.H., Lee, J.S., Lee, H.Y., Jin, K.M., Heo, C.-H., and Hong, Y.-K., 2011, Evaluation of development possibility for the security of industrial mineral resources (Cu, Pb, Zn, Au etc.) on the domestic mines. GP2010-024-2011(2), Korea Institute of Geoscience and Mineral Resources (KIGAM), Daejeon, 33–216 p.

Chi, S.J., Kang, I.-M., Kim, E.-J., Kim, I.J., Park, S,-W., Lee, J.H., Lee, H.Y., Jin, K.M., Heo, C.-H., Hong, Y.-K., and Lee, J.S., 2012, Evaluation of development possibility for the security of industrial mineral resources (Cu, Pb, Zn, Au etc.) on the domestic mines. GP2010-024-2012(3), Korea Institute of Geoscience and Mineral Resources (KIGAM), Daejeon, 27–88 p.

Clark, R.N., 1999, Chapter 1: Spectroscopy of Rocks and Minerals, and Principles of Spectroscopy. In: Rencz, A.N. (ed.), Manual of Remote Sensing, Volume 3, Remote Sensing for the Earth Sciences. John Wiley and Sons, New York, p. 3–58.

Clark, R.N., Swayze, G.A., Wise, R., Livo, E., Hoefen, T., Kokaly, R., and Sutley, S.J., 2007, USGS digital spectral library splib06a: U.S. Geological Survey, Digital Data Series, 231 p. http://speclab.cr.usgs.gov/spectral.lib06

Hauff, P.L., 2008, An overview of VIS-NIR-SWIR field spectroscopy as applied to precious metals exploration. Spectral International Inc., 80001, 303–403.

Herrmann, W., Blacke, M., and Doyle, M., 2001, Short wavelength infrared (SWIR) spectral analysis of hydrothermal alteration zones associated with based metal sulfide deposits at Rosebery and Western Tharsis, Tasmania, and Highway-Reward, Queensland. Economic Geology, 96, 939–955.

Hinchey, J.G., 2011, Visible/infrared spectroscopy (VIRS) of volcanogenic massive sulfide hydrothermal alteration products, Tulks volcanic belt, Central NewFoundland: An additional exploration technique? Geological Survey, Report, 11-1, 97–108.

Hwang, D.H., 1997, Metallogeny, Geochemistry and mineral exploration of Wondong mine area in Taebaegsan mineralized province, Korea. Ph.D. Thesis, Kyungpook National University, Daegu, 282 p. (in Korean with English abstract)

Hwang, D.H. and Lee, J.Y., 1998, Ore genesis of the Wondong polymetallic mineral deposits in the Taebaegsan metallogenic province. Economic and Environmental Geology, 31, 375–388. (in Korean with English abstract)

Jeong, Y.S., Yu, J.H., Koh, J.-M., and Heo, C.-H., 2014, Spectroscopy of skarn in Dangdu Pb-Zn deposit and assessment of skarn exploration approaches employing portable spectrometer. Journal of Mineralogical Society of Korea, 27, 135–147. (in Korean with English abstract)

Kerr, A., Rafuse, H., Sparkes, G., Hinchey, J., and Sandeman, H., 2011, Visible/infrared spectroscopy (VIRS) as a research tool in economic geology: background and pilot studies from NewFoundland and Labrador. Geological Survey, Report, 11-1, 145–166.

Lee, J.-H., 2011, The results of drilling in Weondong mine area, the Taebaegsan mineralized district, Republic of Korea. Economic and Environmental Geology, 44, 313–320. (in Korean with English abstract)

Meinert, L.D., Dipple, G.M., and Nicolescu, S., 2005, World skarn deposits. In: Hedenquist, J.W., Thompson, J.F.H., Goldfarb, R.J., and Richards, J.P. (eds.), Economic Geology 100th Anniversary Volume. Society of Economic Geologists, Littleton, p. 299–336.

Ninomiya, Y., 2002, Mapping quartz, carbonate minerals, and mafic-ultramafic rocks using remotely sensed multispectral thermal infrared ASTER data. Proceedings of SPIE 4710, Thermosense XXIV, 191 (March 15, 2002). doi:10.1117/12.459566

Ninomiya, Y. and Fu, B., 2002, Quartz Index, Carbonate Index and SiO_2 Content Index Defined for ASTER TIR Data. Journal of Remote Sensing Society of Japan, 22, 50–61.

Ninomiya, Y., 2003a, Rock type mapping with indices defined for multispectral thermal infrared ASTER data: case studies. Remote Sensing for Environmental Monitoring, GIS Applications, and Geology II, SPIE, 4886, 123–132.

Ninomiya, Y., 2003b, Advanced remote lithologic mapping in ophiolite zone with ASTER multispectral thermal infrared data. Proceedings of the International Geoscience and Remote Sensing Symposium, 3, 1561–1563.

Ninomiya, Y. and Fu, B., 2010, Regional scale lithologic mapping in western Tibet using ASTER thermal infrared multispectral data. International Archives of the Photogrammetry, Remote Sensing and Spatial Information Science, 38, 454–458.

Park, C.Y., Song, Y.G., Chi, S.J., Kang, I.M., Yi, K.W., and Chung, D.H., 2013, U-Pb(SHRIMP) and K-Ar age dating of intrusive rocks and skarn minerals at the W-skarn in Weondong deposit. Journal of Mineralogical Society of Korea, 26, 161–174. (in Korean with English Abstract)

Pontual, S., Gamson, P., and Merry, N., 2012, Spectral interpretation field manual: Spectral Analysis Guides for Mineral Exploration, G-Mex Version 3.0. Ausspec International Propriety Limited, Australia, Vol. 1, 191 p.

Rowan, L.C. and Mars, J.C., 2003, Lithologic mapping in the Mountain Pass, California area using advanced spaceborne thermal emission and reflection radiometer (ASTER) data. Remote sensing of Environment, 84, 350–366.

Son, Y.S., Kang, M.K., and Yoon, W.J., 2014, Lithological and mineralogical survey of the Oyu Tolgoi region, Southeastern Gobi, Mongolia using ASTER reflectance and emissivity data. International Journal of Applied Earth Observation and Geoinformation, 26, 205–216.

Sonntag, I., Laukamp, C., and Hagemann, S.G., 2012, Low potassium hydrothermal alteration in low sulfidation epithermal systems as detected by IRS and XRD: An example from the Co-O mine, Eastern Mindanao, Philippines. Ore Geology Reviews. 45, 47–60.

Merry, N., Pontual, S., and Gamson, P., 1999, The Spectral Geologist "TSG" v 2.0 user manual. AusSpecInternational Pty. Ltd. 136 p.

Sun, Y., Seccombe, P.K., and Yang, K., 2001, Application of short-wave infrared spectroscopy to define alteration zones associated with the Elura zinc-lead-silver deposit, NSW, Australia. Journal of Geochemical Exploration, 73, 11–26.

Thompson, A.J.B., Hauff, P.L., and Robitaille, A.J., 1999, Alteration mapping in exploration: application of short-wave infrared (SWIR) spectroscopy. Society of Economic Geology Newsletter, 39, 16–27.

Whitney, D.L. and Evans, B.W., 2010, Abbreviations for names of rock-forming minerals. American Mineralogist, 95, 184–187.

Yang, K., Huntington, J.F., Browne, P.R.L., and Ma, C., 2000, An infrared spectral reflectance study of hydrothermal alteration minerals from the Te Mihi sector of the Wairakei geothermal system, New Zealand. Geothermics, 29, 377–392.

Yang, K., Browne, P.R.L., Huntington, J.F., and Walshe, J.L., 2001, Characterising the hydrothermal alteration of the Broadlands-Ohaaki geothermal system, New Zealand, using short-wave infrared spectroscopy. Journal of Volcanology and Geothermal Research, 106, 53–65.

Zadeh, M.H., Tangestani, M.H., Roldan, F.V., and Yusta, I., 2014, Spectral characteristics of minerals in alteration zones associated with porphyry copper deposits in the middle part of Kerman copper belt, SE Iran. Ore Geology Reviews, 62, 191–198.

Manuscript received May 23, 2015
Manuscript accepted July 6, 2015